

Dynamic Drop Simulation of the Main Landing Gear of a General Aviation Aircraft

Ning Li¹, Han Wang², Zhiqiang Li^{2,3,4} & Zhihua Wang^{1,3,4}

¹Taiyuan University of Technology, College of Mechanical & Vehicle Engineering, Taiyuan 030024, China
 ²Taiyuan University of Technology, College of Aeronautics & Astronautics, Jinzhong 030600, China
 ³ Shanxi Key Laboratory of Material Strength and Structural Impact, Taiyuan University of Technology, Taiyuan 030024, China

⁴Institute of Applied Mechanics, College of Mechanical and Vehicle Engineering, Taiyuan University of Technology, Taiyuan 030024, China

Abstract

More than half of aircraft accidents occur during takeoff and landing phases, underscoring the critical importance of the landing gear as a load-bearing component. Despite the widespread use of leaf-spring landing gears in light aircraft due to their simplicity and reliability, challenges persist in handling the dynamic loads during landing, which significantly affect gear performance. Traditional design practices often simplify these dynamic conditions into static problems, potentially compromising the design's effectiveness under extreme conditions. This study presents an advanced methodology for the design and development of landing gear using a dynamic model approach from the preliminary stages. Utilizing the finite element software Abaqus, the research developed a parametric model of the landing gear, incorporating a rigid-flexible coupling analyzed through explicit dynamics to simulate landing impacts. Secondary development via Python scripts enhanced the post-processing capabilities, allowing for detailed data analysis. Integration with Isight software facilitated multi-objective optimization, leading to improvements in buffer efficiency, reduced structural weight, and minimized design and testing costs. This integrative approach exemplifies how advanced modeling and simulation can streamline landing gear development, ensuring safer and more efficient aircraft operations.

Keywords: Landing gear; Finite element analysis (FEA); Dynamic simulation; Multi-objective optimization.

1. Introduction

Over 50% of aircraft accidents occur during the takeoff and landing phases [1]. The landing gear, being an essential load-bearing component during these stages, plays a pivotal role in the safety and performance of the aircraft. Leaf-spring landing gears are extensively used in small and light aircraft owing to their simplicity, reliability, and ease of maintenance [2].

Compared to the static loads experienced while the aircraft is parked, the dynamic loads encountered during landing exert a more substantial impact on the performance of the landing gear and its associated components. Consequently, these dynamic loads are a critical factor in the strength verification process of the landing gear [3]. However, in the design process of fixed landing gear, engineers often rely on experience to simplify the load conditions during landing and braking, transforming complex multibody dynamics problems into static problems [4]. This simplification can lead to excessive design margins, thereby reducing the rationality of the design. Additionally, this approach may overlook the potential negative impacts of complex loads under extreme conditions on structural strength, buffer performance, and the stability and durability of the system.

The design and development of landing gear is a repetitive, iterative process that aims to achieve an optimal balance among strength, stiffness, and weight [5]. Consequently, the design and production cycle for landing gear is lengthy, prototype testing is costly, and drop tests pose significant risks [6]. Establishing a dynamic model for leaf spring landing gear at the preliminary design stage and developing a scientifically sound multi-objective optimization method are therefore crucial. This approach not only substitutes for initial drop tests but also provides technical guidance for subsequent experiments, effectively shortening the design cycle, enhancing design efficiency, reducing costs, and maximizing the rationality of the design.

In 2015, Krason and Malachowski used LS-DYNA to conduct both static and dynamic analyses of a flexible three-dimensional model of landing gear components. This analysis considered the interactions between oil, gas, the internal structure of the landing gear, and the contact issues between flexible wheels and the ground, thereby validating the effectiveness of the finite element model [7]. In 2018, Zhang B and colleagues utilized the simulation software ANSYS CFX for the numerical simulation of a landing device for an unmanned underwater glider, aiming to explore potential enhancements in optimization goals through the response surface methodology and particle swarm optimization [8]. In 2020, Srivathsa and Adarsha developed a two-degree-of-freedom mathematical model of the main landing gear, which absorbed the majority of the impact loads. They derived dynamic equations based on this model to analyze the landing dynamics of the main landing gear system [9]. Jianmin Lu conducted a dynamic analysis of the landing gear using ANSYS. investigating the mechanical characteristics of the landing gear's shock absorber under various compression strokes and landing deflection angles through a single-factor method [10]. In 2021, Pirooz and Mirmahdi proposed a novel method to control the dynamic response of the landing gear during heavy landings or taxiing [11]. Sonowal and Pandey performed a finite element analysis on the landing gear damping model of the large commercial jet Boeing 787-8, thereby validating the mechanical performance of the landing gear constructed from high-strength stainless steel [12].

The research content mentioned above primarily focuses on oil-gas type landing gear, with very limited studies and optimization efforts directed towards spring-type landing gear.

This study uses the conceptual design model of a multi-purpose general aviation aircraft's landing gear as an example. It simplifies the landing gear and related airframe structures reasonably, ensuring they accurately reflect the structural force transmission characteristics and geometric features. Using the Part module in the finite element analysis software Abaqus, a parametric model of the landing gear was designed. A rigid-flexible coupling relationship was then established through the Interaction module. Subsequently, an explicit dynamics analysis step was employed to simulate the landing impact scenario of the landing gear, from which data on buffering characteristics and structural strength were obtained. Furthermore, secondary development of the post-processing module in Abaqus was performed using Python scripts, which enabled the extraction, processing, and analysis of extensive simulation data. Finally, the simulation optimization software Isight integrated Abaqus, the Python scripts, and the batch scripts driving the Python scripts, achieving a coupled simulation. This process facilitated the parametric optimization and automated iteration of the leaf-spring landing gear, not only significantly enhancing the buffering efficiency and reducing the structural weight but also shortening the design cycle and lowering experimental costs.

2. Aircraft Basic Parameters

This type of general aviation aircraft has a maximum takeoff weight W_{TO} = 1180 kg and is designed for a maximum sink speed of 8.7 ft/s, equivalent to V_{sink} = 2.65 m/s.

The overall design geometric parameters of the landing gear are as follows: main wheel base is 2470 mm, the distance from front wheel to the main wheels F = 2190 mm, and the center of gravity height $H_{CG} = 1310$ mm, with an tipback angle $\beta = 15^{\circ}$.

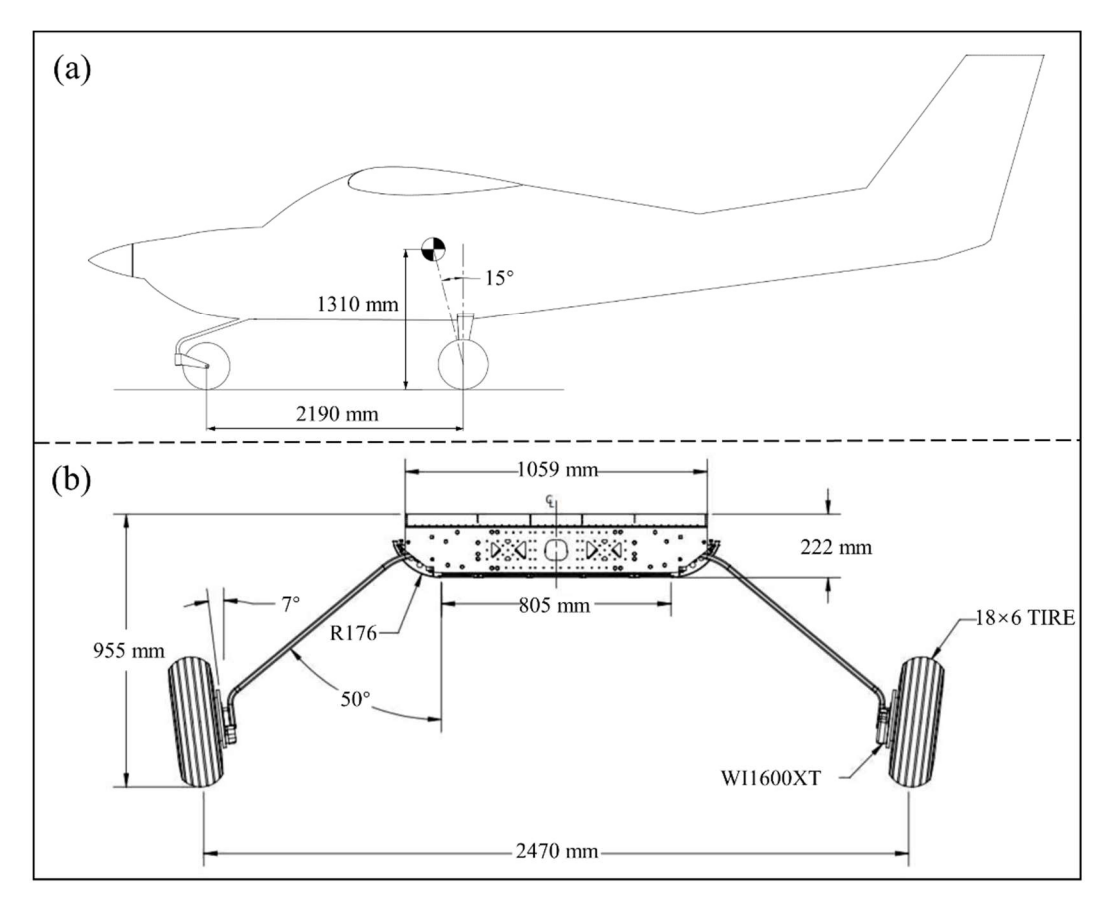


Figure 1 – Engineering drawing: (a) aircraft and (b) landing gear.

3. Landing Gear Shock Absorption Theoretical Analysis

The landing gear's shock-absorbing buffer system is utilized during landings and while maneuvering on uneven runways to absorb and dissipate shock energy, thus bearing the loads applied to the gear. The impact energy A during landing is dependent on the aircraft's landing weight W_L and the vertical sink speed V_{sink} . It will be absorbed by the buffer system in the form of deformation energy A_{def} . For general aircraft, V_{sink} is 3.0 m/s to 4.0 m/s. For each group of nose and main landing gear buffer system, should absorb the energy:

$$A_{def} = \frac{1}{2} W_L \left(V_{sink} \right)^2 \tag{1}$$

After the aircraft touches down, the force exerted by the runway surface on the tires $\sum P_k$ during a downward displacement of the center of gravity H_{CG} determines the value of A_{def} , expressed as:

$$A_{def} = \int_0^{H_{CG}} \sum P_k dH = \frac{1}{2} W_L (V_{sink})^2 = PH_{CG}$$
 (2)

Where P is the average value of $\sum P_k$, which is the load acting on the aircraft wheel when the aircraft center of gravity shifts from 0 to H_{CG} :

$$PH_{CG} = \frac{1}{2}W_L \left(V_{sink}\right)^2 \tag{3}$$

It can be seen that the greater the displacement of the aircraft's center of gravity H_{CG} during landing, the smaller the load exerted on the landing gear structure.

In the analysis of landing gear shock absorption, the maximum landing weight required is determined in accordance with the Federal Aviation Regulations Part 23. The regulation stipulates that the design

landing weight can be as low as 95 percent of the maximum weight, expressed as:

$$M_{land} = W_{TO} \times 95\% = 1120 \, kg$$
 (4)

The overload of the landing gear is defined as the ratio of the maximum vertical load experienced by the landing gear upon ground contact to its static load. This can be expressed as:

$$n = \frac{P_{\text{max}}}{G} \tag{5}$$

In the equation:

n is the landing gear overload factor.

 P_{max} is the maximum vertical load.

G is the static load experienced by the landing gear when the aircraft is stationary on the tarmac.

The energy absorbed by the landing gear, denoted as W_1 , is calculated as the integral of the ground reaction force over the compression stroke of the landing gear. This represents the work done by the vertical ground load P_{ν} , indicating the energy absorbed by the landing gear in the vertical direction. It is defined as follows:

$$W_1 = \int_0^s P_{\nu} ds \tag{6}$$

The buffer efficiency of the landing gear can be defined as the ratio of the absorbed energy W_1 to the product of the maximum vertical load P_{max} and the maximum compression stroke. This ratio reflects the capability of the landing gear to absorb shock energy, and is expressed as follows:

$$\eta = \frac{W_1}{P_{max}S_{max}} \tag{7}$$

In the equation:

 η represents the buffer efficiency of the landing gear.

 S_{max} is the maximum compression stroke of the landing gear.

4. Preprocessing for FEA

4.1 Parametric Modeling of Landing Gear

The main landing gear of this type of aircraft consists of left and right leaf spring assemblies, symmetrically arranged about the aircraft's plane of symmetry. This paper focuses on modeling and analysis of the left-side leaf spring assembly.

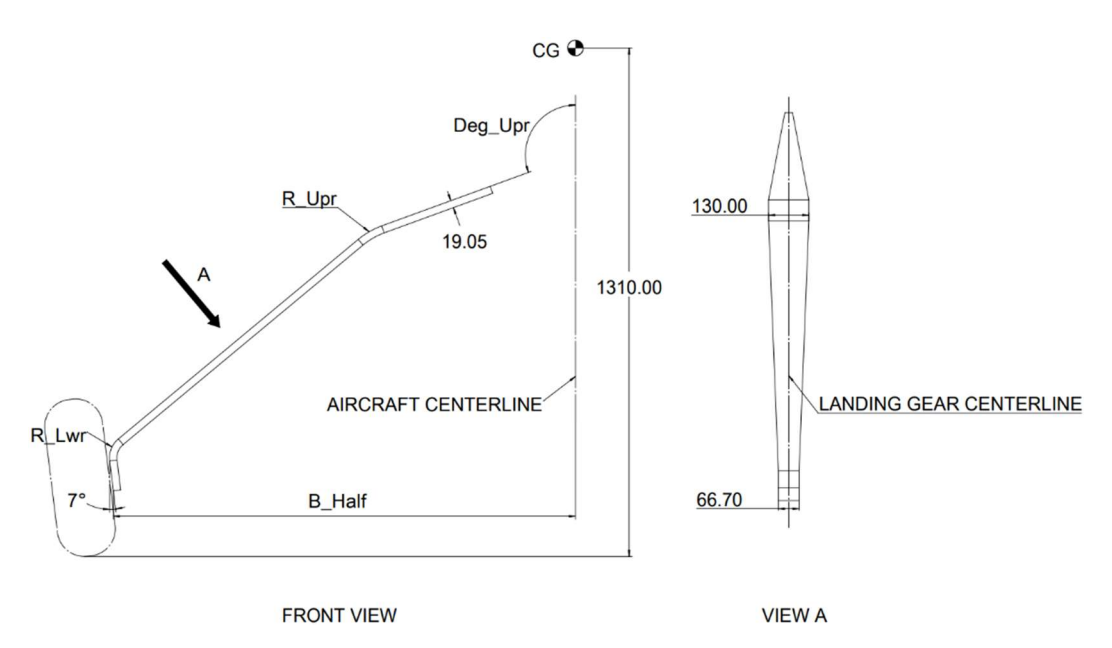


Figure 2 – Diagram of the parametric modeling of landing gear.

This paper involves the design of a parametric model. By establishing reasonable sketch constraints and selecting appropriate geometric feature points, lines, and surfaces as references and geometric benchmarks for the sketches, automatic iteration and rapid regeneration of specific dimensions of the leaf spring were achieved. This design cleverly addresses the limitations of the Abaqus assembly module in constraint command options, thereby not only standardizing and automating the entire model construction process but also enhancing the efficiency and accuracy of modeling. Moreover, it lays the foundation for the integration of numerical optimization algorithms and the automatic adjustment of parameters.

Fixed parameters in the parametric model include: the height of the aircraft's center of gravity, the distance between the front and main wheels, tire camber angle, the relative position between the tire model and the outer mounting surface of the lower leaf spring, the shape of the lower leaf spring, and the shape of the connection joints between the landing gear and the airframe (i.e., the shape of the upper leaf spring). Under these conditions, the design variables are as shown in the Table 1 below.

Table 1 – Design Valiables Table.				
Name	Symbol	Current Value	Unit	
Upper Arc Radius	R_Upr	203.20	mm	
Lower Arc Radius	R_Lwr	63.50	mm	
Lateral Extension of Lower Leaf Spring	B_Half	1192.83	mm	
Upper Leaf Spring Installation Angle	Deg Upr	110.00	0	

Table 1 - Design Variables Table

The parameters mentioned above are based on mainstream engineering empirical methods [13]. During the design process, the impact resistance of the landing gear and the strength of the wheel loads are primarily estimated based on the results of static analysis. This approach ensures that the structural integrity and functionality of the landing gear are adequate for operational demands.

The aircraft tire model is constructed based on the outer mounting surface of the lower leaf spring and uses two geometric features of the leaf spring as reference points in the sketch. Therefore, when the design variables are modified, the tire will only shift in its lateral position, while its ground clearance remains unchanged. This ensures that the tire's position relative to the ground remains consistent during operation, irrespective of changes to other design parameters.

4.2 Material Properties

The material used for the landing gear leaf springs is modified 6150 chrome vanadium steel, which has

undergone specific heat treatment. The material properties are detailed in Table 2.

Table 2 – Material properties of 6150 chrome vanadium steel.

Material Properties	Value	Unit	Material Properties	Value	Unit
Elasticity Modulus	190	GPa	Poisson's Ratio	0.29	
Tensile Strength	1.76	GPa	Density	7800	kg/m³
Yield Strength	1.62	GPa			

To simplify the finite element analysis, the ground model is set as an analytical rigid body. This configuration allows for the output of reaction force data at the reference node of the rigid ground, which represents the wheel load data.

The mass of the landing gear model was measured in Abaqus as $M_{model} = 0.0280$ t, with the mass of the leaf spring being $M_{leaf} = 0.0174$ t (units consistent with those used in Abaqus).

4.3 Mesh Generation

The finite element model of the landing gear underwent mesh generation. The global element size (Seed Part Instance) was set to 6.1 mm to ensure that at least three elements were included in the thickness direction of the leaf spring. In the regions where the landing gear connects to the aircraft fuselage structure, swept meshing was employed to avoid excessively large aspect ratios. A detailed geometric subdivision was performed for the tire model, achieving a fully structured mesh. Seed edges were individually set for the edges of the tire contact zone, with an edge mesh size of 10 mm. The entire model comprised 72380 nodes and 64106 elements, discretized using linear hexahedral elements of type C3D8R.

4.4 Deformability of Aircraft Tire

In dynamic simulations, contact between rigid tires and a rigid ground often leads to computed wheel load values significantly higher than actual values. This can also result in repeated oscillations between the tire and the ground, leading to discontinuities in the wheel load curve. Therefore, it is important to consider the elastic properties of the tire and model it as a deformable body in the simulation. To simplify the calculation process, this study employed a linear model to describe the behavior of the aviation tire.

This study referenced tire parameters from a single-engine, four-seat general aviation aircraft with a maximum takeoff weight of 1080 kg and a tricycle landing gear configuration. According to international standards for low-pressure aviation tires, the deflection rate typically falls between 31% and 36%, resulting in a calculated deflection of 42.5 mm [14]. In preliminary explicit dynamic simulations, the wheel load was found to be 16.75 kN, as reflected in the data output of the preliminary simulations. To achieve a deflection of 42.5 mm in the tire finite element model, a trial-and-error method was employed to adjust the elastic modulus of both the tire contact area and transition area. This adjustment was made to ensure consistency with the wheel load determined from the preliminary simulations.

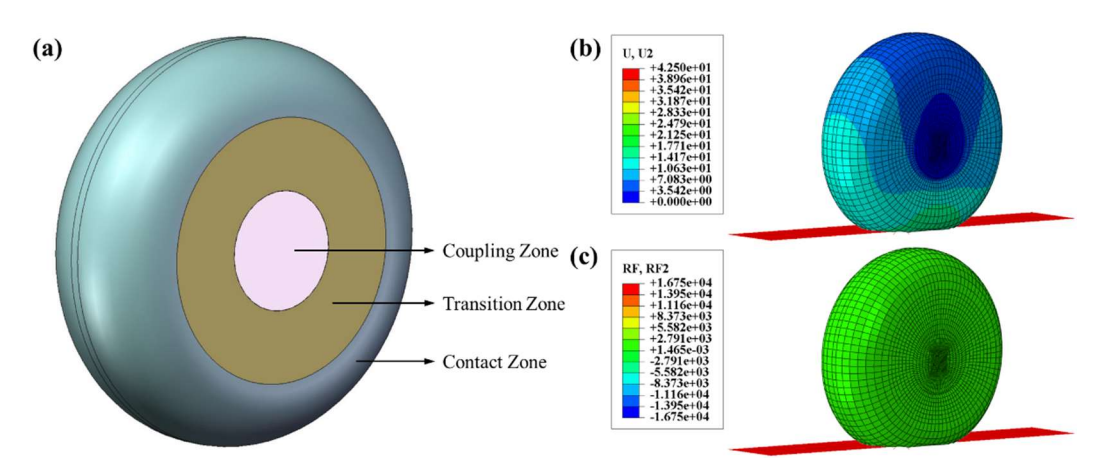


Figure 3 – Deformability of aircraft tire: (a) tire region segmentation; (b) deformation and (c) reaction force distribution plot.

4.5 Interaction Definition

The leaf spring does not possess energy-dissipating capacity. Therefore, in aircraft equipped with leaf spring landing gear, the dissipation of landing kinetic energy primarily relies on the friction between the tires and the ground. In this study, a friction coefficient of 0.5 was set [15].

A reference point was created at the center of gravity position, named RP-CG. Geometric subdivisions were applied to the upper leaf spring, delineating the areas connected to the aircraft fuselage structure. A kinematic coupling was employed between these areas and RP-CG to simulate the effect of the landing gear connected to the fuselage structure via bolts. Additionally, kinematic couplings were also applied to the coupling zones on both sides of the tire and the outer mounting surface of the lower leaf spring.

The results of mesh generation and interaction processing are shown in Figure 4.

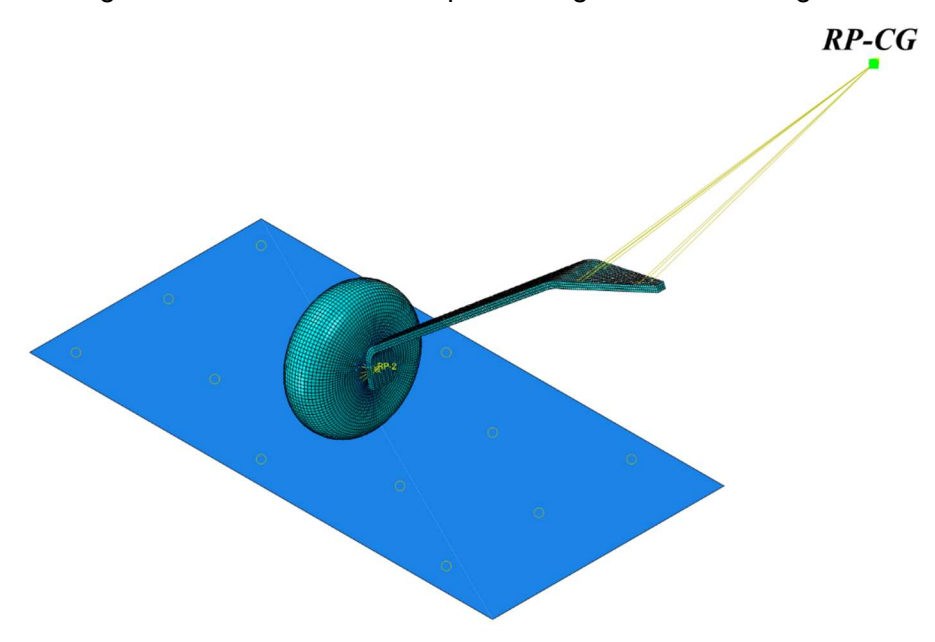


Figure 4 – Mesh and interactions

5. Static Analysis

5.1 FEA Analysis Steps

To ensure effective convergence in contact calculations, the ground was lifted by 0.5 mm to achieve

contact with the tires in Step-1 by modifying the boundary conditions. Subsequently, in Step-2, the ground was fixed in place, and a vertical downward load was applied to the reference point RP-CG.

5.2 Static Loads Calculation

Based on the aircraft's basic parameters and landing gear configuration, the static load during parking is calculated as $G = W_T \times (F - M) / (2F) = 495$ kg, equivalent to 4855.21 N.

5.3 Analysis Results

The finite element analysis results are shown in Figure 5 and Figure 6.

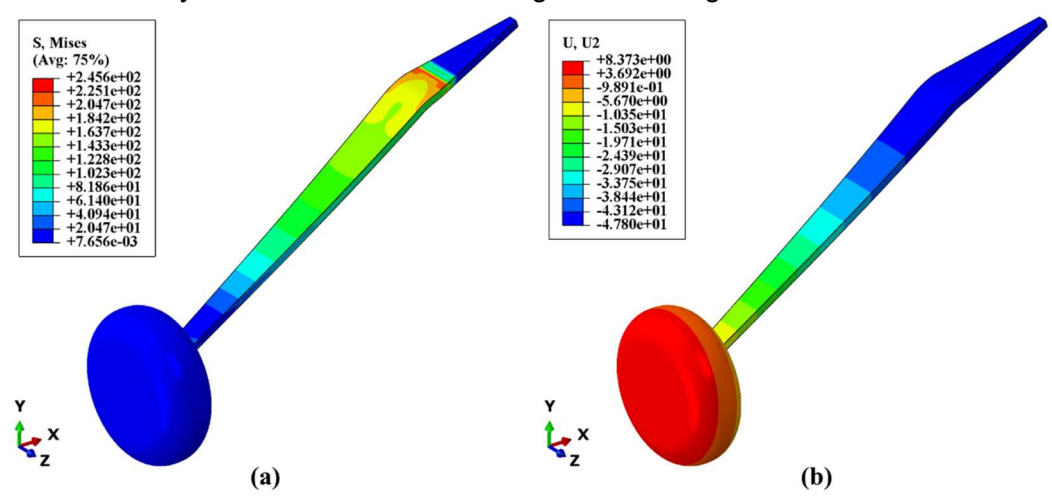


Figure 5 – Static analysis result: (a) stress distribution and (b) deformation.

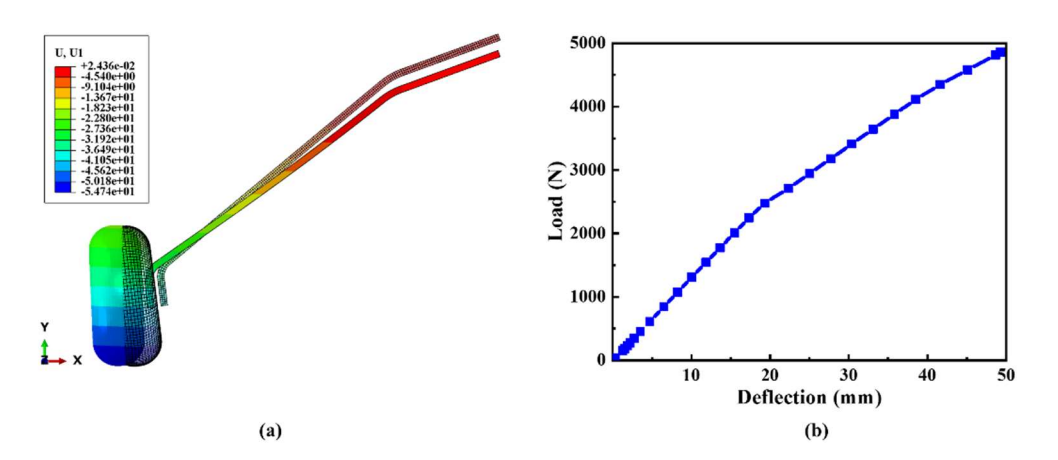


Figure 6 – Static analysis result: (a) deformation in front view and (b) load-deflection curve. Under the full load condition of 1180 kg during parking, the maximum stress in the structure is 245.60 MPa, meeting the strength requirements of the metallic material. The maximum stress is located at the connection between the landing gear and the fuselage, which is in accordance with engineering practice. The maximum deflection is 47.8 mm, and the maximum extension (lateral displacement) is 54.7 mm. At this point, the main wheel attitude is favorable, complying with relevant specifications for landing gear structural design [4].

5.4 Summary

This chapter has preliminarily validated the correctness of the kinematic coupling and contact settings in the Interaction module through static analysis. The initial stress levels are relatively low, demonstrating the rationality of the selected material properties and boundary condition settings. This provides a reliable basis for the subsequent dynamic simulations.

6. Dynamic Analysis

6.1 FEA Analysis Steps

Analysis Step: An explicit dynamic analysis step was created to simulate the dynamic behavior of the landing gear under the maximum landing weight and symmetric landing conditions of the aircraft. Due to the bending of the landing gear leaf spring structure with increasing load, resulting in a decrease in the moment arm and entering a nonlinear state, the geometric nonlinearity option (NIgeom On) was enabled in Abagus.

Time Period: During the landing impact process of the leaf spring landing gear, multiple cycles of compression and rebound occur, stabilizing after several repetitions. Moreover, the maximum compression occurs during the initial landing impact, and the most severe landing overload also occurs at this time [16]. Therefore, this study primarily analyzes the first landing impact process.

6.2 FEA Model Setup

Interaction, geometric models, mesh generation, and material properties are consistent with the static analysis.

6.3 Dynamic Loads and Boundary Conditions

Aircraft Mass: RP-CG was set as an inertia mass point, with a value of half of the maximum landing weight minus the landing gear model mass, i.e., $M_{inertia} = 1/2 \times M_L - M_{model} = 532.19$ kg.

Lift and Gravity Acceleration: Vertical lift is applied at RP-CG, with a value of 2/3 of the maximum landing weight [13]. Gravity is applied at 9.8 m/s², providing the landing gear and mass point with a vertical velocity of 2.65 m/s to simulate their collision with the ground.

6.4 Analysis Results

The output results of the explicit dynamic analysis are shown in the following figures.

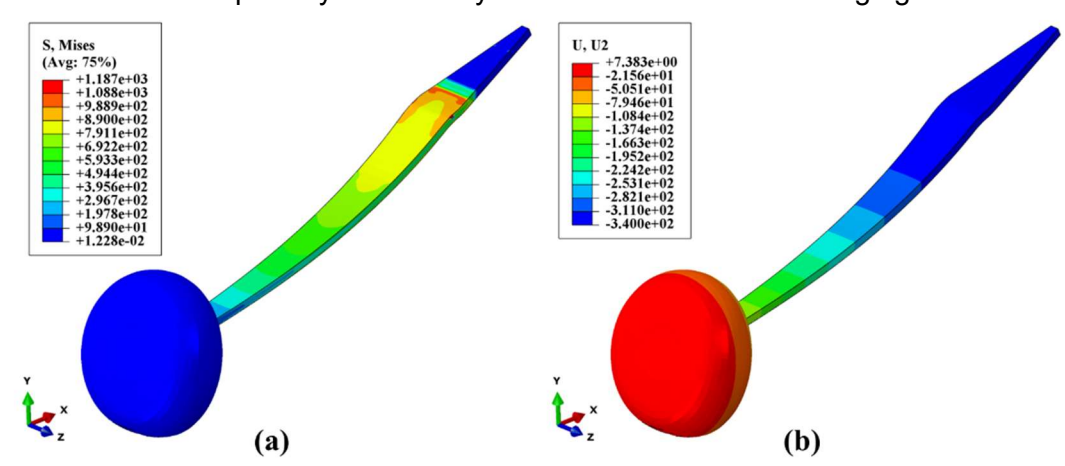


Figure 7 – Dynamic analysis result: (a) stress distribution and (b) deformation.

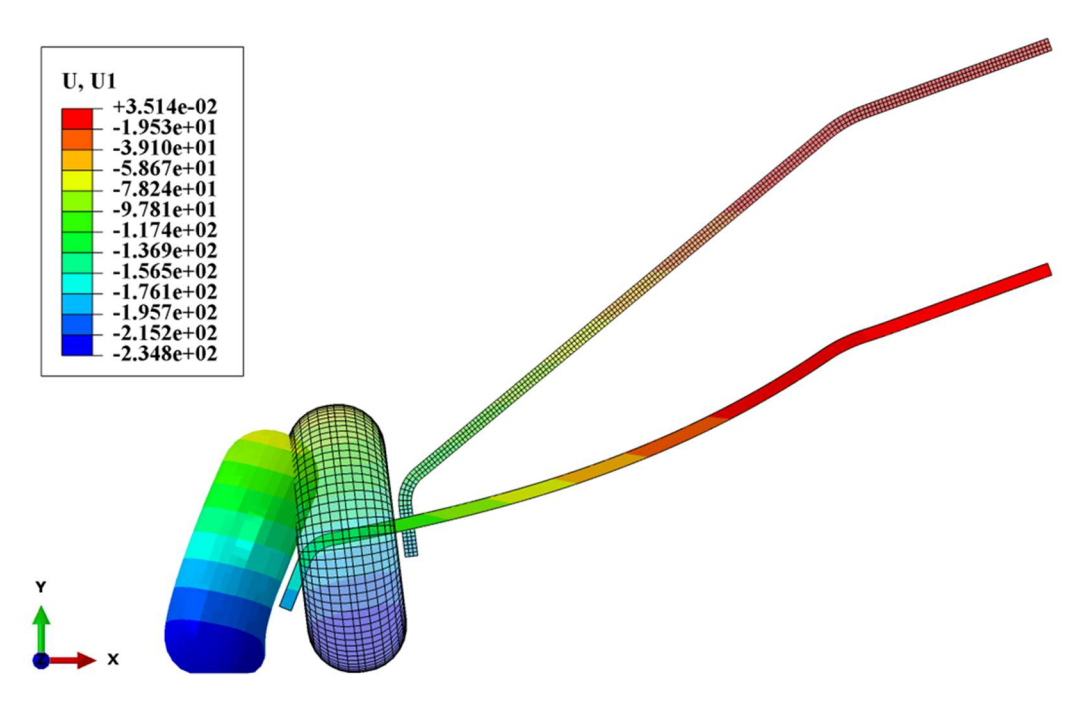


Figure 8 – Deformation in front view.

The buffer characteristic curve is shown in Figure 9.

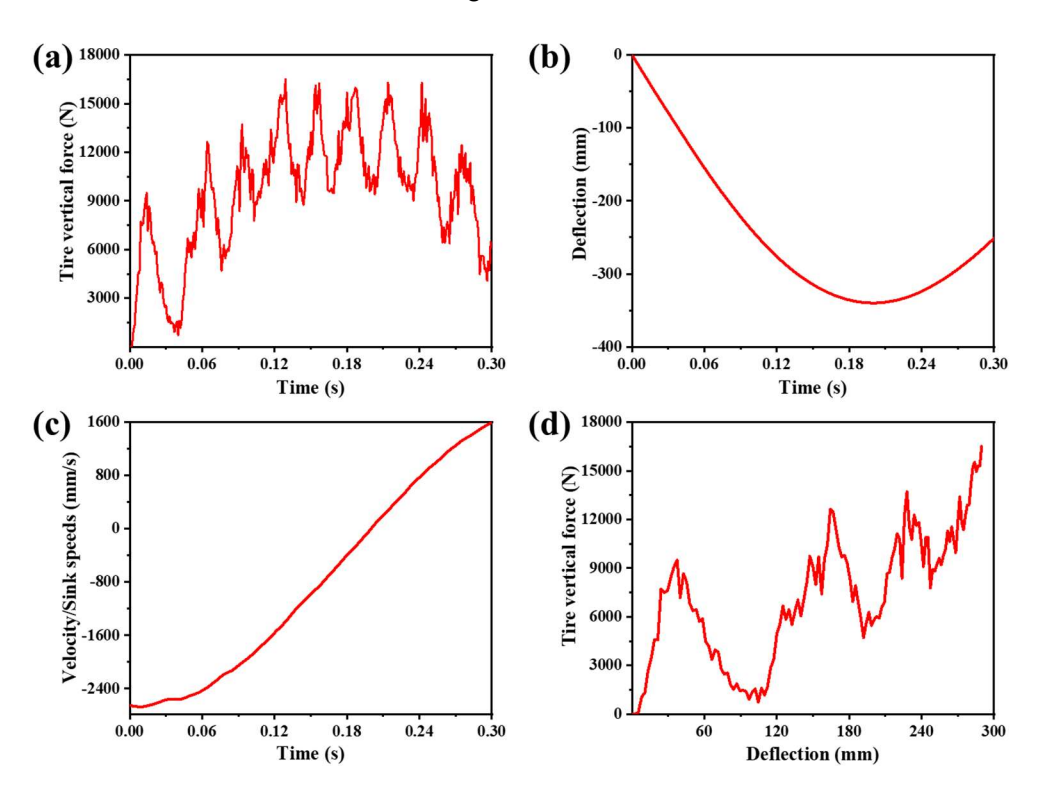


Figure 9 – Buffer characteristic curve: (a) tire vertical force-time curve; (b) deflection-time curve;

(c) sink speed-time curve and (d) tire vertical force-deflection curve.

Under the landing impact condition, the buffer characteristic curve conforms to the practical engineering trend. The maximum stress in the structure is 1186.70 MPa, meeting the strength requirements of the metal. The location of the maximum stress is consistent with the parking condition, located at the connection between the landing gear and the fuselage. The maximum vertical wheel load $P_{max} = RF2_max = 16505.80$ N, corresponding to the maximum landing overload n = 3.40, and the landing gear efficiency n = 0.40.

The phenomenon of severe fluctuations in wheel loads curves over a short period of time can be attributed to several factors: (1) Low stiffness of the leaf spring and the substantial weight of the tire result in larger deformation and oscillation at the ends under the action of inertial forces, leading to more significant deformation and oscillation. (2) The dynamic loading during landing is a complex multi-degree-of-freedom system problem. The aircraft's longitudinal, lateral, and vertical motions impose forces and moments on the landing gear in different directions. The superposition of these forces and moments generates complex oscillation modes. (3) The nonlinear behavior of the leaf spring under large deformation is another significant factor causing oscillations. Both geometric and material nonlinearity make oscillations more complex and intense, especially under extreme conditions, where nonlinear effects significantly influence the amplitude and frequency of oscillations. (4) Inaccurate material models contribute to the oscillations. The inherent damping properties of tire materials affect the rate of vibration attenuation. Insufficient damping leads to prolonged oscillations.

6.5 Hourglass Energy Check

Energy output is an important part of an ABAQUS/ Explicit analysis. Comparisons between various energy components can be used to evaluate whether an analysis is yielding an appropriate response. Large values of artificial strain energy indicate that significant elemental distortions (i.e. defined as hourglassing phenomena in finite element analysis) have occurred and a mesh refinement is necessary to be done. We can diagnose hourglassing through optical inspection of the mesh deformation, adjusting its scale factor as needed. However, the most reliable method is to directly compare the energy contained in the zero energy modes (hourglass energy) with the internal energy of the system. In the finite element analysis, the artificial strain energy for the whole model (ALLAE) includes energy stored in hourglass resistances, transverse shear in shell and beam elements. It is generally recommended that the artificial strain energy should be less than 10% of its internal energy for the whole model (ALLIE) [17].

This comparison is achieved by plotting the energies from historical data.

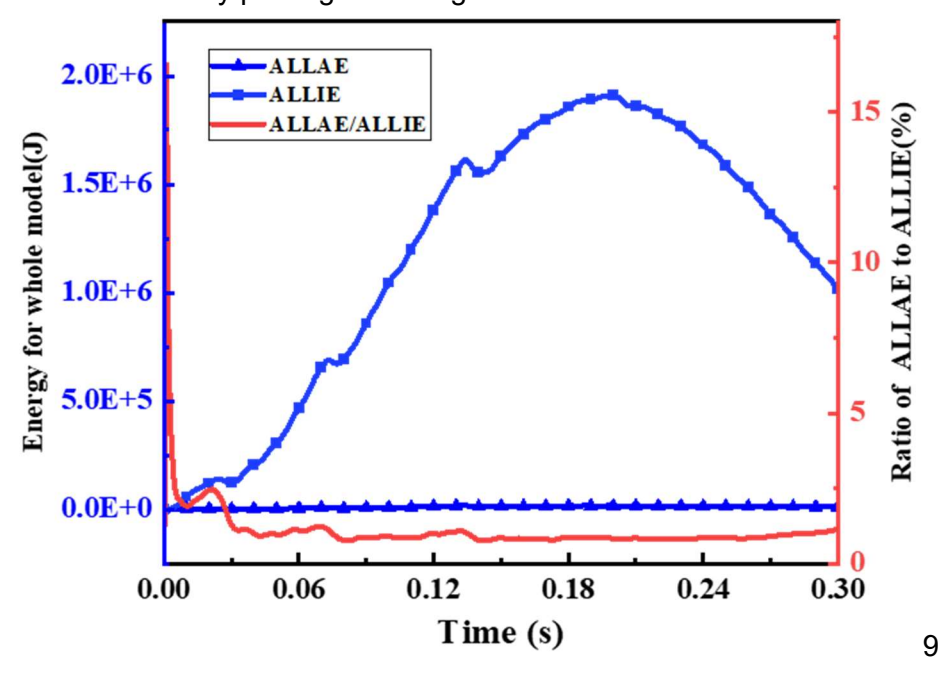


Figure 10 – Hourglass energy check.

As shown in Figure 10, during the early stages of the landing impact process, the ratio reaches a maximum value of 16.57%. However, at this point, the tire has not fully contacted the ground, and the model has not undergone significant deformation. Therefore, the transient value at this stage is a result of dividing one number by another very small number and cannot serve as a basis for judging the occurrence of hourglassing phenomena.

After this stage, the ratio of ALLAE to ALLIE remains well below 5% at all times, indicating that the hourglass mode has a minimal effect on the computed results of this study, thus validating the

rationality and accuracy of the simulation model.

After 0.3 seconds, the external forces acting on the tire will gradually diminish, and the strain energy will be released as work, causing the deformable bodies to return to their original state, rendering the ratio irrelevant for reference.

6.6 Summary

In this chapter, explicit dynamic analysis was conducted to obtain the buffer characteristic curves of the leaf spring landing gear. The reliability and accuracy of the dynamic simulation model were ensured through hourglass energy check. This preparation lays the groundwork for the subsequent multi-objective optimization using the validated dynamic simulation model.

7. Multi-Objective Optimization Based on Isight

In this study, secondary development of the post-processing module in Abaqus was conducted through using Python scripts. Batch processing commands (.bat files) were utilized to drive the execution of Python scripts, enabling automatic extraction, processing, and analysis of dynamic simulation data.

7.1 Python Code Development

Specifically, Python code was employed to extract all reaction force (tire vertical force) data RF2 and vertical displacement (landing gear compression stroke) data U2 from the analysis step until the maximum reaction force value $RF2_max$ in the entire data sequence was obtained. The corresponding displacement data was ensured to match the same number of data points as the reaction force data. Then negated once to ensure all displacement data were positive. The extracted data was then integrated using Simpson's rule to obtain the integral value W_1 . The landing gear buffer efficiency η was calculated as:

$$\eta = \frac{W_1}{RF2_max \times U2_max} \tag{8}$$

Finally, the buffer efficiency was outputted as a .txt document named 'Efficiency.txt', containing the efficiency value and all *RF2* and *U2* data involved in the integration calculation.

The method for calculating buffer efficiency is based on Simpson's rule, which approximates integrals using quadratic curves instead of rectangular or trapezoidal integration formulas, resulting in higher approximation accuracy. Simpson's rule is relatively simple and practical in engineering calculations [18].

7.2 Isight-Driven Integrated Simulation and Optimization

Lastly, the simulation optimization software Isight was integrated with Abaqus, Python scripting programs, and batch processing commands to achieve joint simulation—optimization.

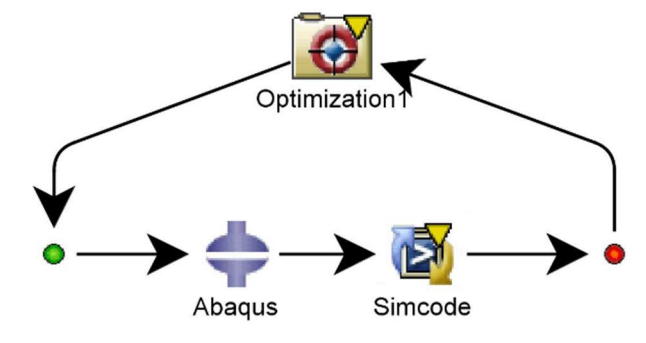


Figure 11 – Isight simulation–optimization workflow diagram.

Isight is a generic software framework for integration, automation, and optimization of design processes that has been developed on the foundation of interdigitation: the strategy of combining multiple optimization algorithms to exploit their desirable aspects for solving complex problems. With

the recent paradigm shift from traditional optimization to design space exploration for evaluating "whatif" scenarios and trade-off studies, Isight has grown from an optimization software system to a complete design exploration environment, providing a suite of design exploration tools including a collection of optimization techniques, design of experiments techniques, approximation methods, and probabilistic quality engineering methods. Likewise, the interdigitation design methodology embodied in Isight has grown to support the interdigitation of all design exploration tools for effective design space exploration [19].

lsight has been widely used in the field of mechanical design for its ability to quickly improve product performance and effectively reduce design costs [20].

7.2.1 Design Variables

According to Table 1, the selected design variables are parameters R Upr, R Lwr, B Half, Deg Upr.

$$X = [R_Upr, R_Lwr, B_Half, Deg_Upr]$$
 (9)

7.2.2 Constraints

According to the aircraft design manual, the requirement for the roll angle θ of runway aircraft should not exceed 63° [21]. Therefore, the range of B_Half is set as follows: $980 \le B_Half \le 1400$. This corresponds to a roll angle range of $52^\circ \le \theta \le 60^\circ$.

Other constraints can be expressed as:

$$\begin{cases} \lambda \sigma_m \le \sigma_s \\ U_1 \le X \le U_2 \end{cases} \tag{10}$$

where λ is the safety factor, taken as 1.2 [22]. σ_m is the maximum stress during the landing gear shock absorption process. σ_s is the allowable stress of the material. U_1 and U_2 are the upper and lower limits of the design variables, determined comprehensively based on aircraft overall design, experience in the design of leaf spring landing gear structures, and material physical properties.

7.2.3 Objective Function

The objective function aims to minimize the mass of the leaf spring landing gear, maximize the buffer efficiency, and minimize the wheel load.

$$\begin{cases}
\min\{m(X)\} \\
\max\{e(X)\} \\
\min\{rf(X)\}
\end{cases}$$
(11)

7.2.4 Optimization Algorithm

The Non-Dominated Sorting Genetic Algorithm II (NSGA-II) was employed in Isight for optimizing the leaf spring landing gear.

When there are multiple optimization objectives, due to the conflicts between the optimization objectives, sometimes one optimization objective is improved, while simultaneously another optimization objective is deteriorated. It is difficult to find a solution that furnishes all the objective functions optimal at the same time. Therefore, it is used to optimize the multi-objective problem by Non-Dominated Sorting Genetic Algorithm II [23,24]. For multi-objective optimization problems, there is usually a set of solutions that cannot be compared between them with respect to the overall objective function. It is characterized by the fact that it is impossible to improve any objective function without weakening at least one other objective function.

The approach to integrated simulation optimization is depicted in the following diagram.

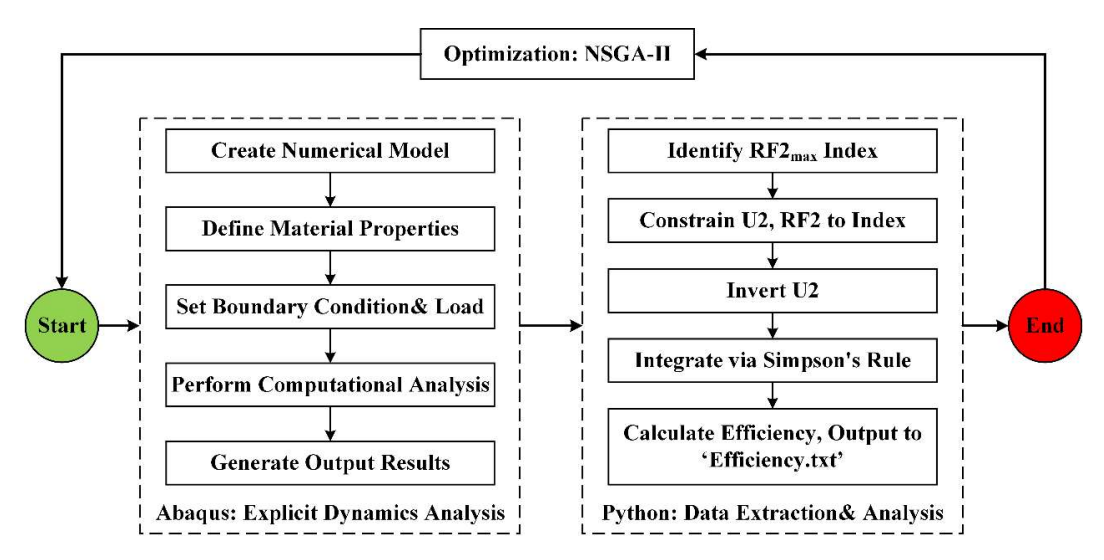


Figure 12 – Integrated simulation optimization workflow diagram.

7.3 Optimization History Analysis

The response of the mass of the leaf spring landing gear (*Mass*) to the number of iterations during the optimization process is illustrated in Figure 13.

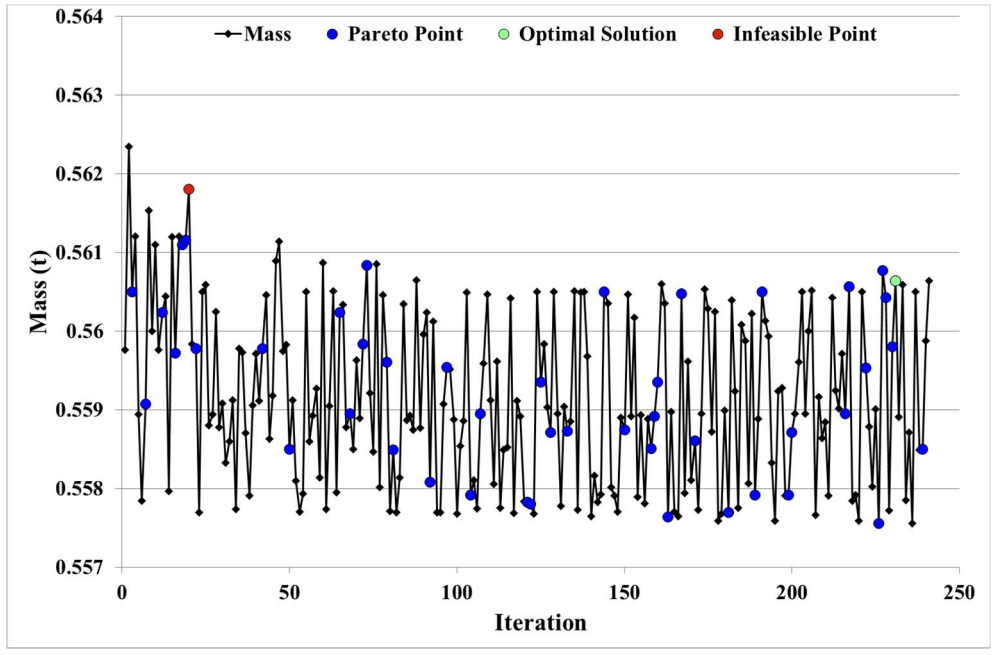


Figure 13 – Landing gear mass optimization history.

Figure 14 displays the response of the efficiency (*Efficiency*) of the leaf spring landing gear buffer over the number of iterations during optimization.

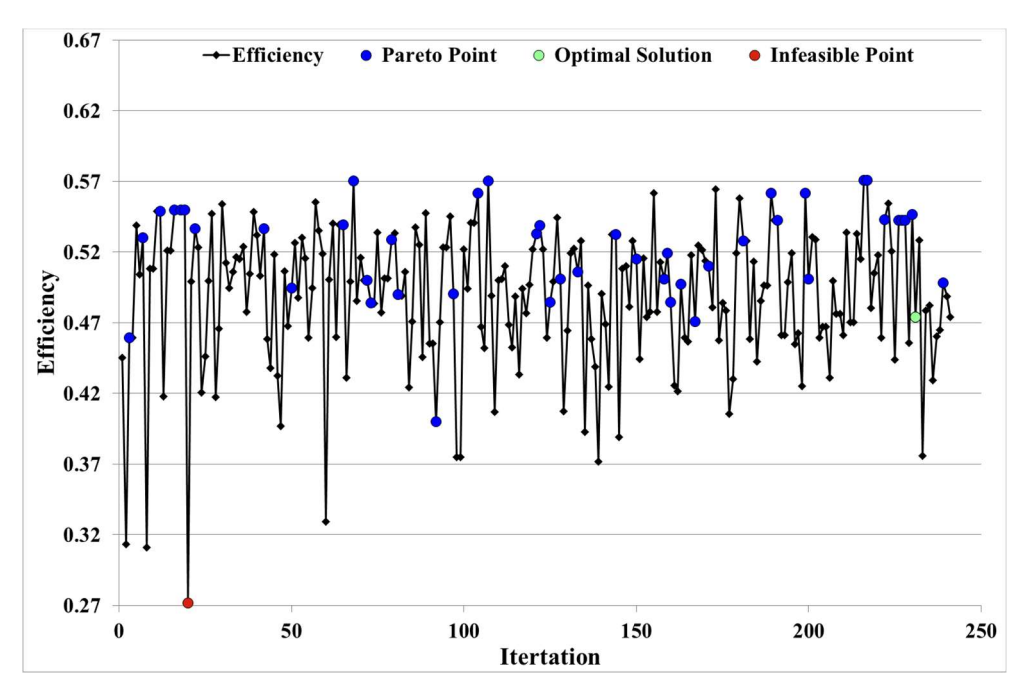


Figure 14 – Landing gear buffer efficiency optimization history.

The variation of the maximum reaction force (RF2_max), representing the wheel load during the landing impact process of the leaf spring landing gear, with the number of iterations, is depicted in Figure 15.

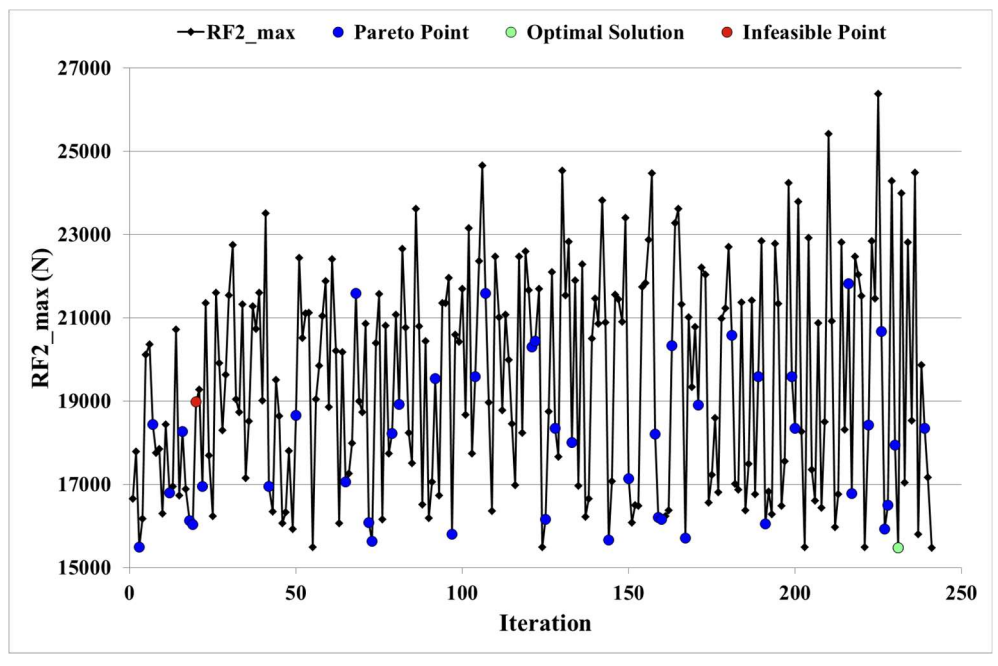


Figure 15 – Maximum tire vertical force optimization history.

Figure 16 demonstrates the response of the maximum equivalent stress (*Mises_max*) of the leaf spring landing gear to the number of iterations during optimization.

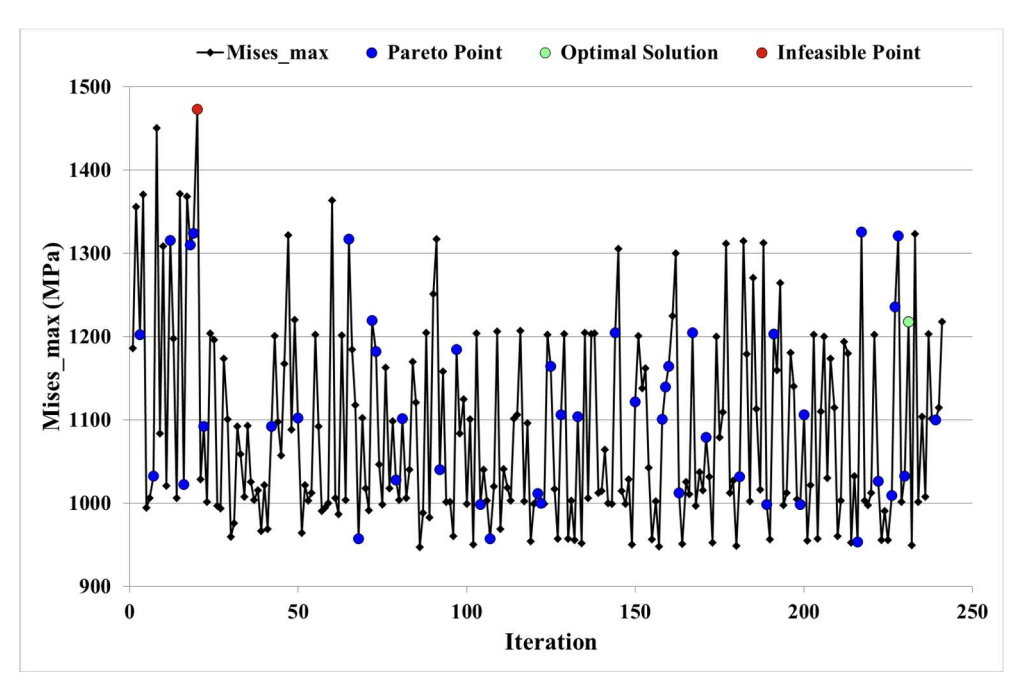


Figure 16 – Response of maximum von mises stress to iteration count.

The black points in Figure 13-16 represent the normal feasible points. Light red represents an infeasible design point, which indicates the actual values that do not satisfy the defined constraints for any parameter. The green point represents the best design point, which is based on the calculated objective. This point is always a feasible point (i.e., no violated constraints). Blue represents a Pareto point. When multiple objectives are defined in the problem formulation, there is no single "best point" but instead a set of points (called the Pareto set) from which tradeoffs can be made. For any one of these points, no improvement can be made in one objective without giving something up in another. A green point is actually also a Pareto point, but it is the one with the best calculated weighted sum objective and penalty value among all of the Pareto points.

The optimization history plots demonstrate a clear convergence trend of the optimization objectives with an increasing number of iterations during this optimization process. Eventually, they stabilize within a consistent range. This indicates that the adopted optimization algorithm effectively guides the objective function to gradually approach a stable solution, proving the effectiveness and convergence performance of the algorithm under the current parameter settings.

The Pareto frontier solutions obtained at the end of the optimization process are depicted in Figure 17.

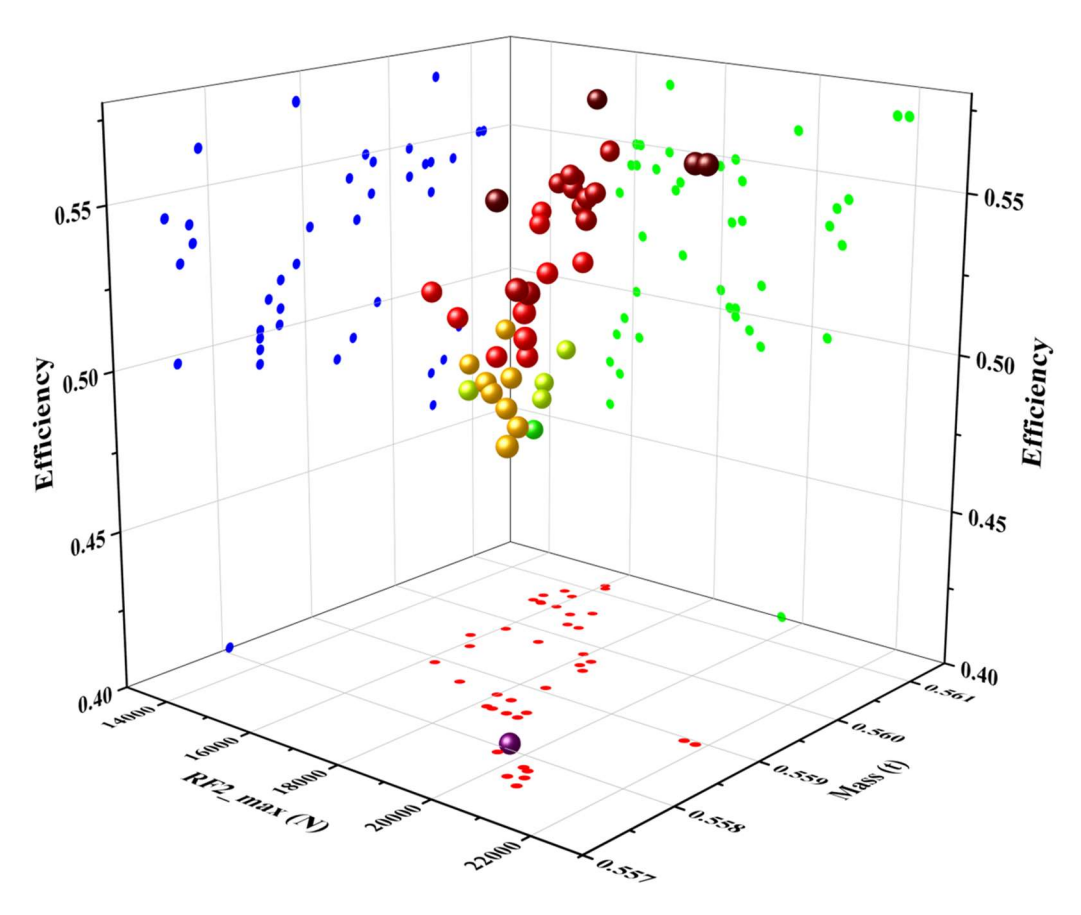


Figure 17 – Pareto frontier solutions.

The 3D scatter plots illustrating the design points relative to the mass of the leaf spring landing gear are shown in Figure 18.

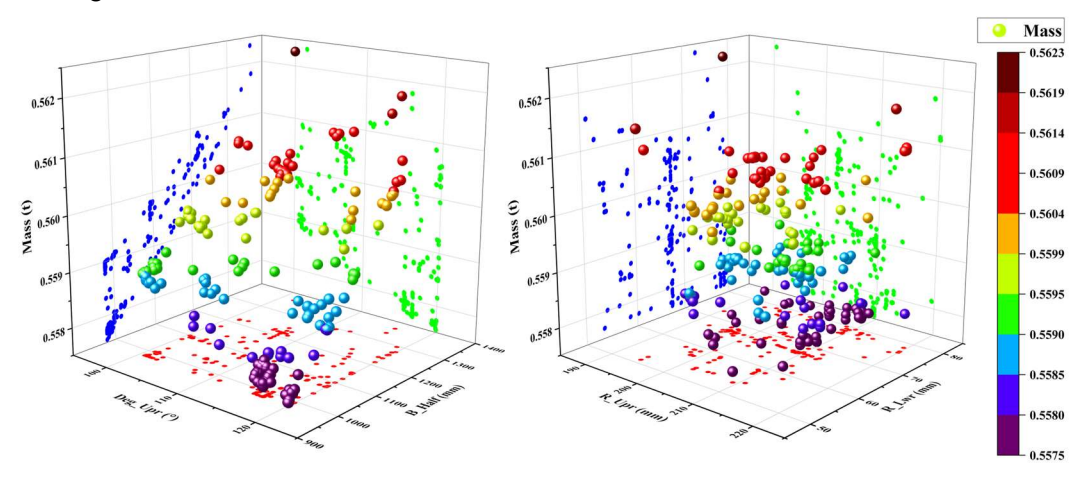


Figure 18 – 3D scatter plot of design points vs. Mass.

Similarly, Figure 19 presents the 3D scatter plots depicting the design points relative to the efficiency of the leaf spring landing gear buffer.

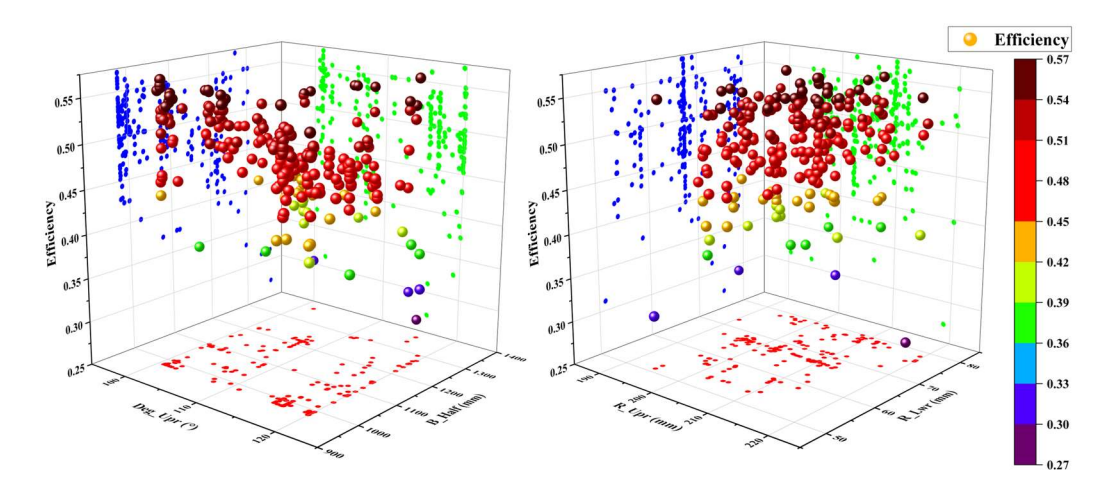


Figure 19 – 3D scatter plot of design points vs. Efficiency.

Furthermore, Figure 20 displays the 3D scatter plots illustrating the design points relative to the maximum reaction force (*RF2_max*) experienced during the landing impact process of the leaf spring landing gear.

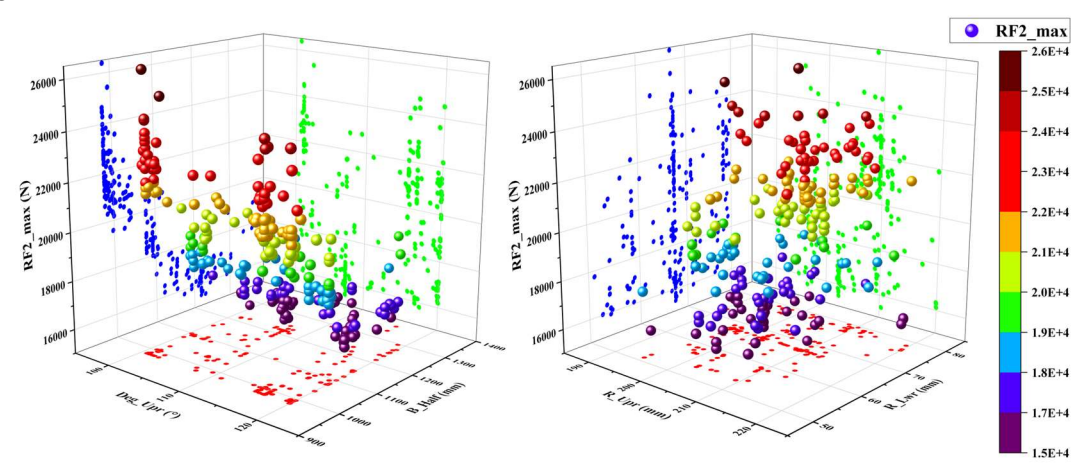


Figure 20 – 3D scatter plot of design points vs. RF2 max.

From Figure 18, Figure 19 and Figure 20, it is evident that the NSGA-II produces numerous design points. Although this may lead to longer computation times, it ensures coverage of the entire design space, making it less prone to local optima. This demonstrates the reliability and effectiveness of the computational results.

A correlation table is a patch chart that uses color to represent the correlation value between selected output parameters and selected input parameters. It provides a quick look at the most influential/influenced parameters from the selected parameters.

The following rank correlation table shows the relationship between the output parameters –maximum von Mises (*Mises_max*), *Mass*, *RF2_max*, and *Efficiency* – and the input parameters, namely *B_Half*, *Deg_Upr*, *R_Lwr*, and *R_Upr*.

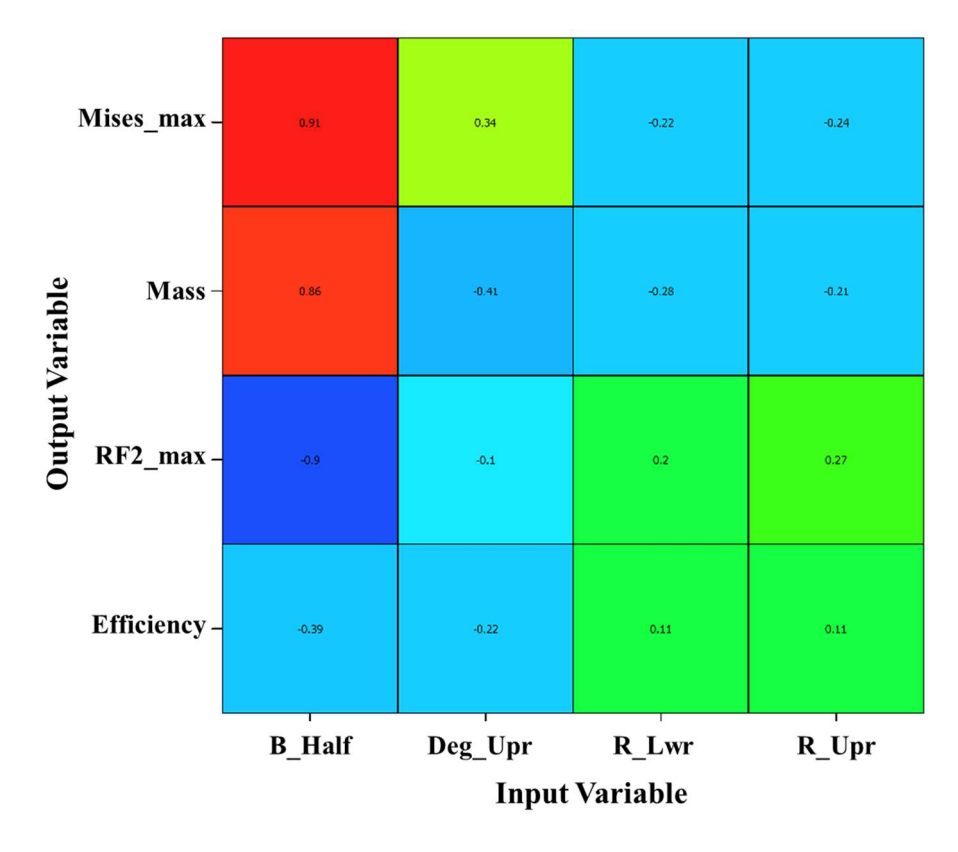


Figure 21 – Correlation table.

The correlation table uses shades of blue, green, yellow, and red to indicate the relationship between parameters. The greater the absolute value of a correlation coefficient, the stronger the relationship is between the parameters. The strongest relationship is indicated by a correlation coefficient of -1 or 1, and the patch is shaded dark blue (-1), dark red (1) red. The weakest relationship is indicated by a correlation coefficient of 0, and the patch is shaded green. Coefficient values between 0 and -1 or 1 are shaded a continuum of blue to green to yellow to red.

In the correlation analysis of the Dynamics Model in Isight using the NSGA-II, key insights can be drawn from the influence of specific design parameters. The *B_Half* shows the most substantial effects, with a strong negative correlation in *Efficiency* (-0.39) and an even stronger negative impact on historical maximum RF2 *RF2_max* (-0.90), while positively influencing *Mass* (0.86) and maximum von Mises stress *Mises_max* (0.91). Conversely, the *R_Upr* generally improves *Efficiency* (0.11) and exhibits a positive effect on *RF2_max* (0.27), but reduces both *Mass* (-0.21) and *Mises_max* (-0.24). The *Deg_Upr* and *R_Lwr* show more mixed effects, with *Deg_Upr* reducing *Mass* significantly (-0.41) and *R_Lwr* showing a mild improvement in *Efficiency* (0.11) and a reduction in *Mises_max* (-0.22).

The analysis provides insights into how changes in specific design parameters influence the efficiency, mass, and stress characteristics. The *B_Half* particularly stands out due to its strong influence on structural stress, leaf spring mass, wheel load and buffer efficiency, and should therefore be prioritized during design. Additionally, an increase in *Deg_Upr* effectively reduces the mass of the leaf spring. However, it also compromises buffer efficiency, which requires a careful evaluation of trade-offs during design considerations. This data is crucial for decision-making in further design optimizations and adjustments.

7.4 Optimization Results

In the Pareto solution set, four Pareto points were selected based on distinct criteria: high buffer efficiency, low landing gear mass, high maximum von Mises stress, and low maximum wheel load. These points were named Iteration 19, Iteration 144, Iteration 227, and Iteration 231, according to their respective iteration numbers. Finite element models of the landing gear were reconstructed for each set of design parameters, and dynamic simulation analyses were performed. The resulting buffer characteristic comparison curves are shown in the following figures.

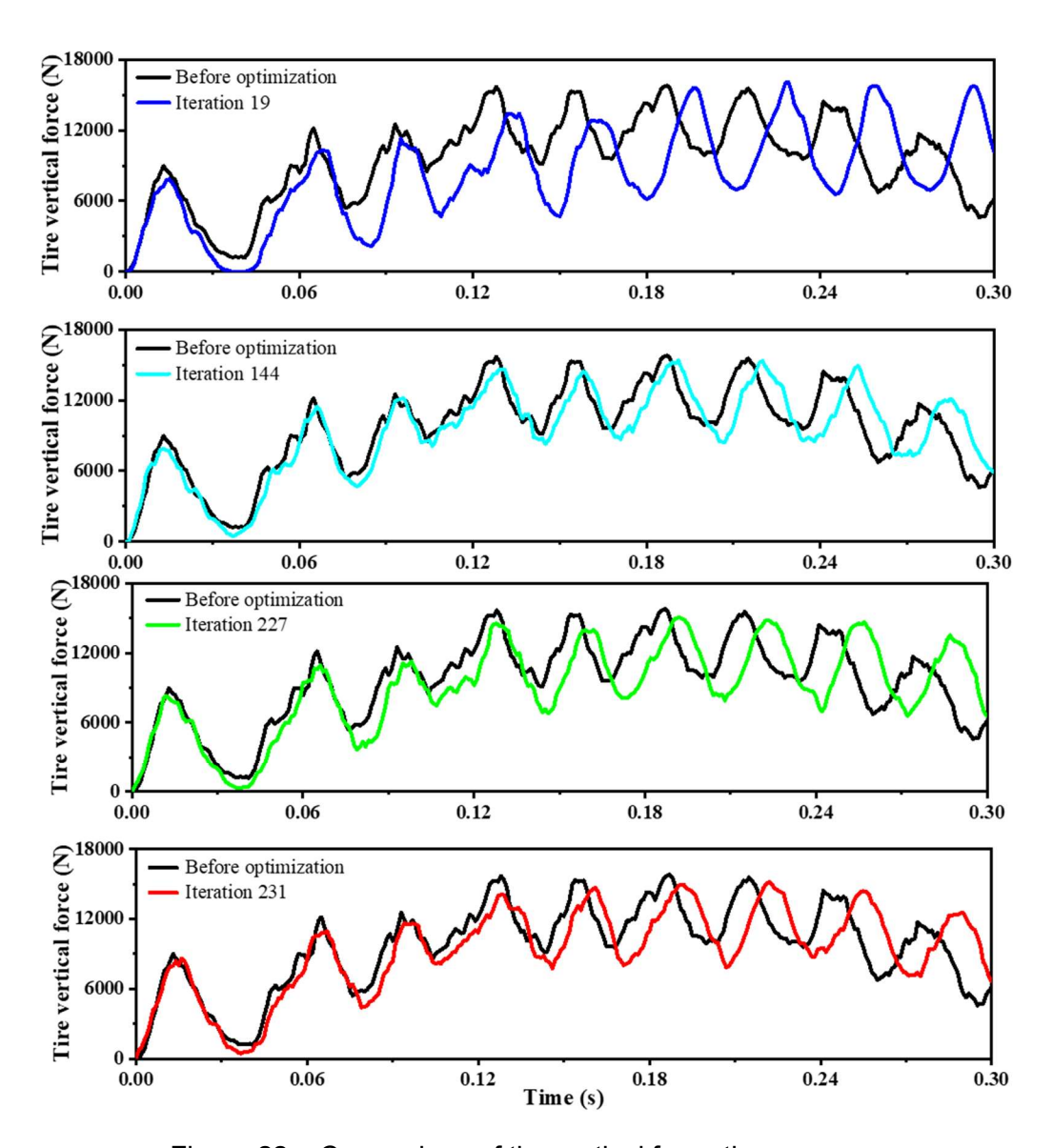


Figure 22 – Comparison of tire vertical force-time curves.

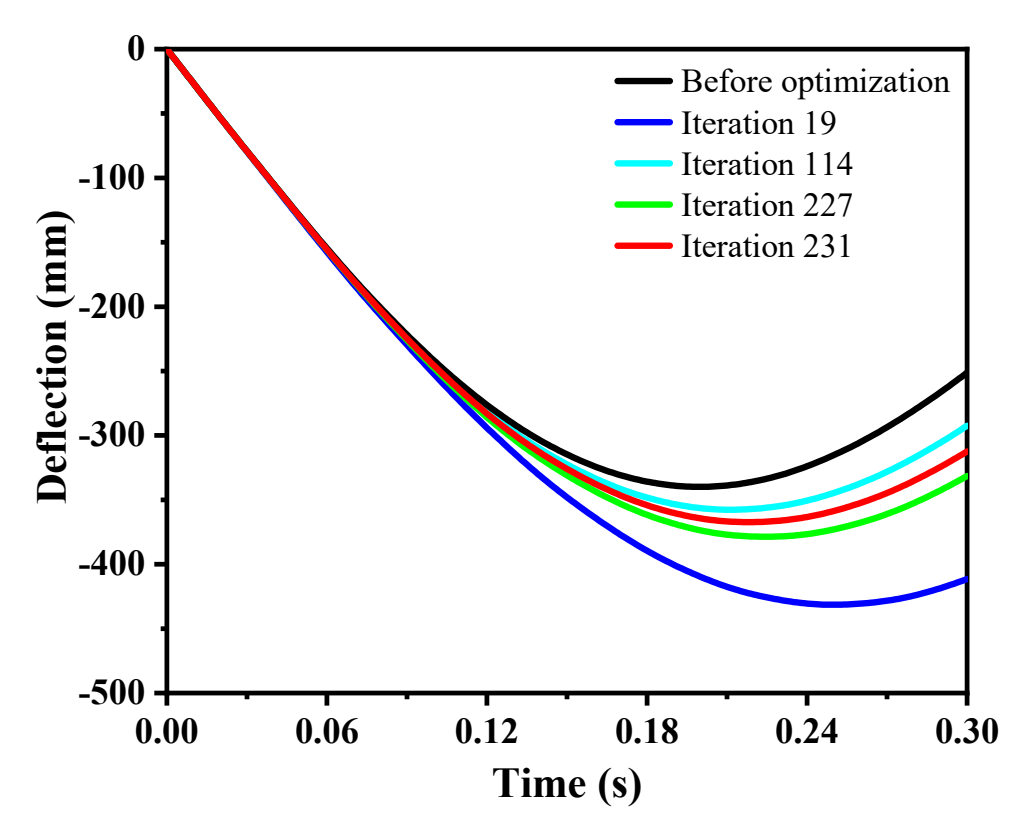


Figure 23 – Comparison of deflection-time curves.

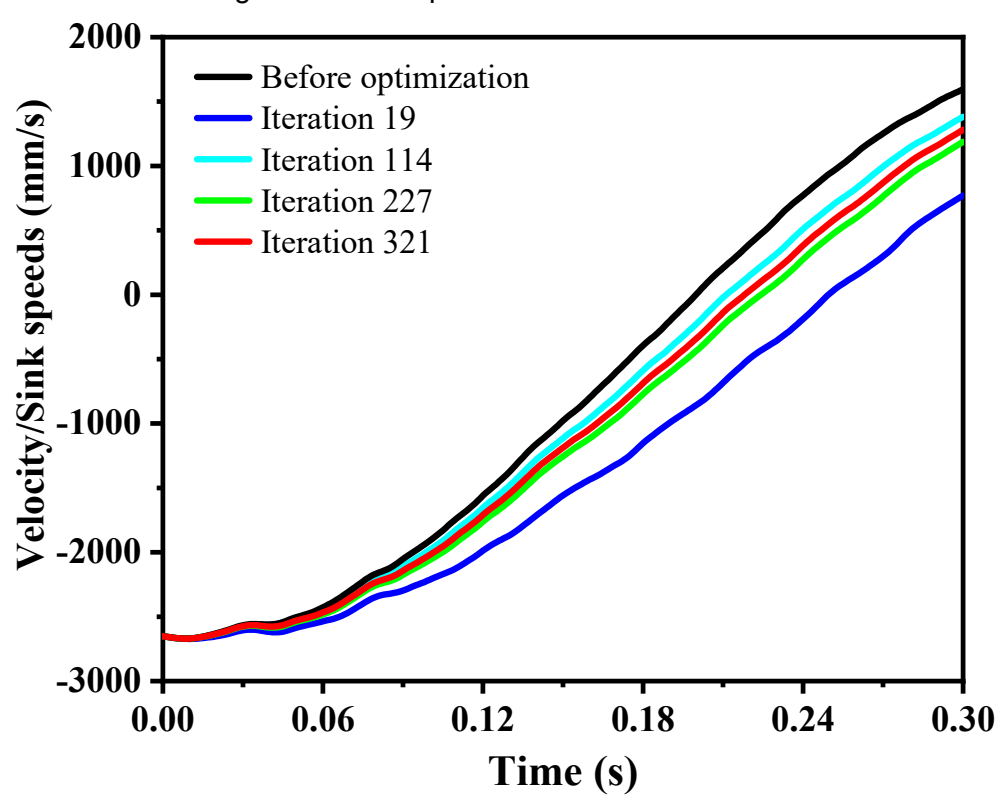


Figure 24 – Comparison of sink speed-time curves.

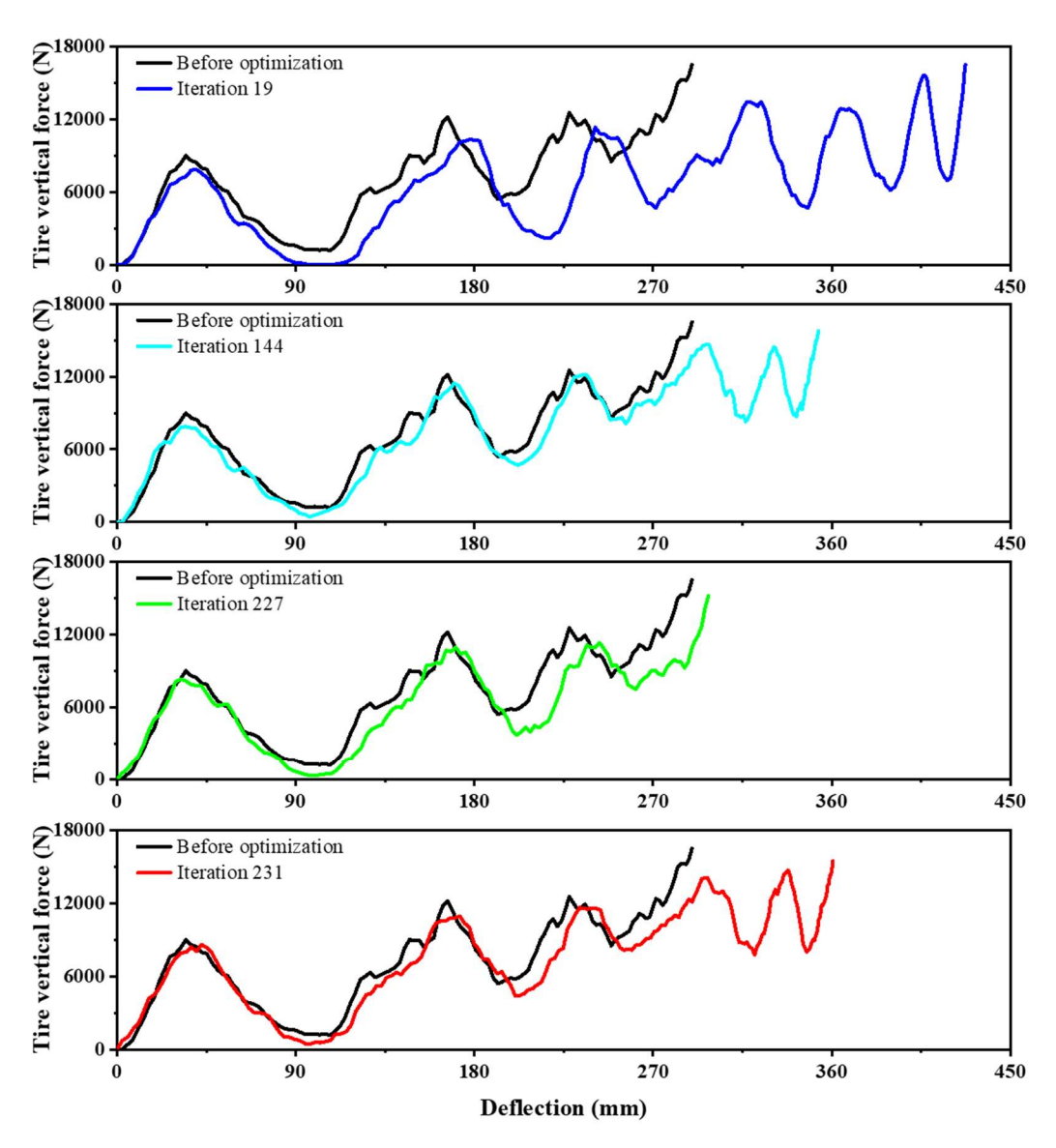


Figure 25 – Comparison of tire vertical force-deflection curves.

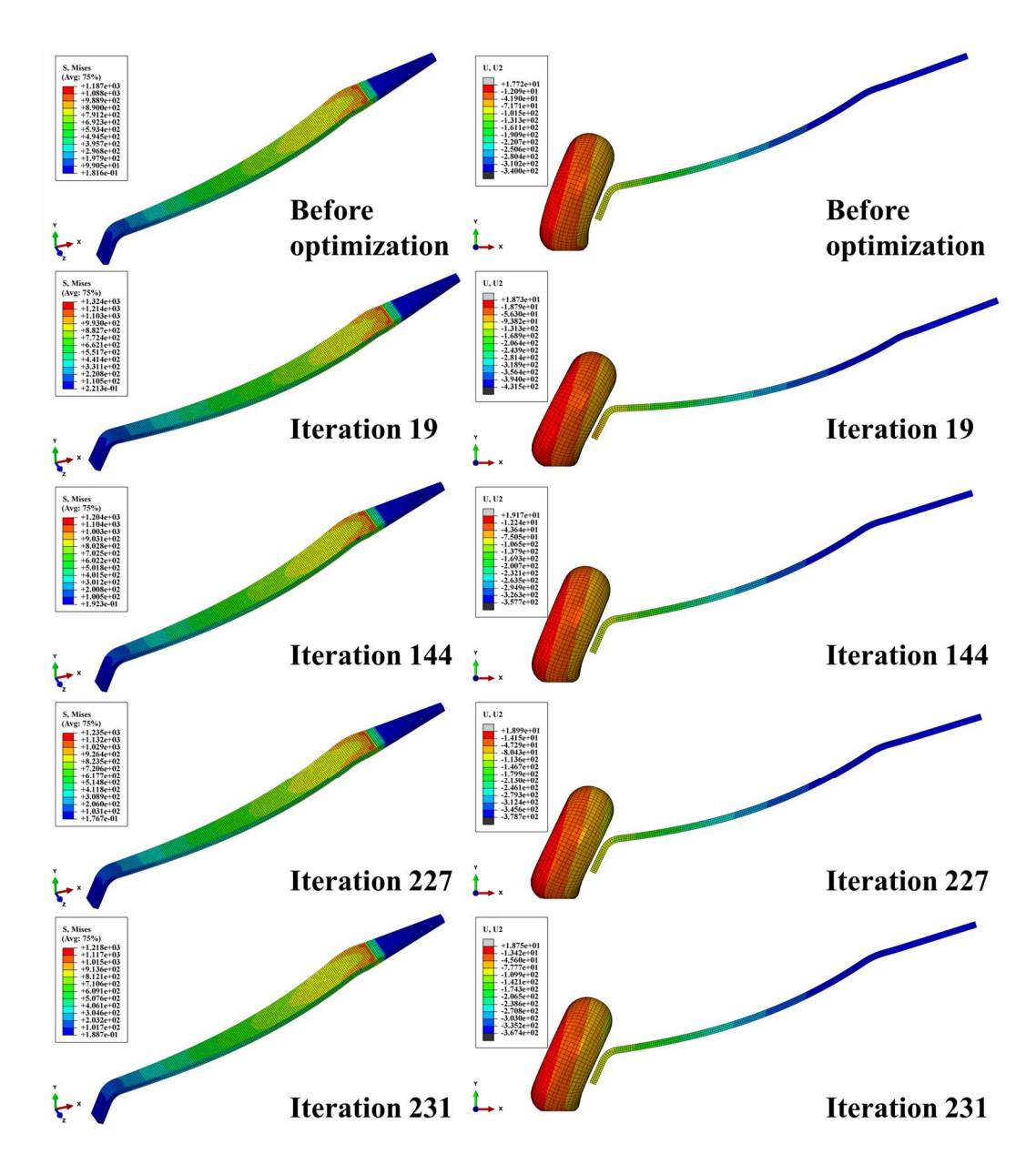


Figure 26 – Contour plots of maximum von Mises stress (left) and maximum deflection (right). In addition to the mentioned data, the buffer efficiency for Iteration 19, Iteration 144, Iteration 227, and Iteration 231 are 0.55, 0.53, 0.54, and 0.47, respectively, all showing significant improvements. The weight of the leaf spring structure is 0.0184 t, 0.0177 t, 0.0180 t, and 0.0178 t, respectively, showing varying degrees of increase.

From the above analysis, it can be seen that the four Pareto frontier solutions in the case led to a partial increase in weight, with specific increases ranging from 0.0003 t to 0.0010 t, corresponding to increases of 1.72% to 5.75%. However, at the same time, the buffer efficiency of the landing gear has been significantly improved, with increases ranging from 17.50% to 37.50%. Overall, the level of wheel load has decreased. The reduction in wheel load reduces the load on the aircraft structure, helping to reduce structural stress and facilitating structural strength optimization and weight reduction design, further improving the overall life and performance of the landing gear.

Taking Iteration 144 as an example, the optimization results are summarized in Table 3.

Table 3 – Optimization results of leaf spring landing gear.

Variables	Initial Value	Range	Result	change
R_Upr (mm)	203.20	190-220	202.37	\

R_Lwr (mm)	63.50	50-80	67.33	\
B_Half (mm)	1192.83	980-1400	1219.12	1
Deg_Upr (°)	110.00	100-120	107.48	\
M _{leaf} (t)	0.0174	\	0.0177	+1.72%
Efficiency	0.40	\	0.53	+32.50%
RF2_max (N)	16505.80	\	15657.10	-5.14%
Mises_max (MPa)	1186.70	\	1204.80	+1.53%

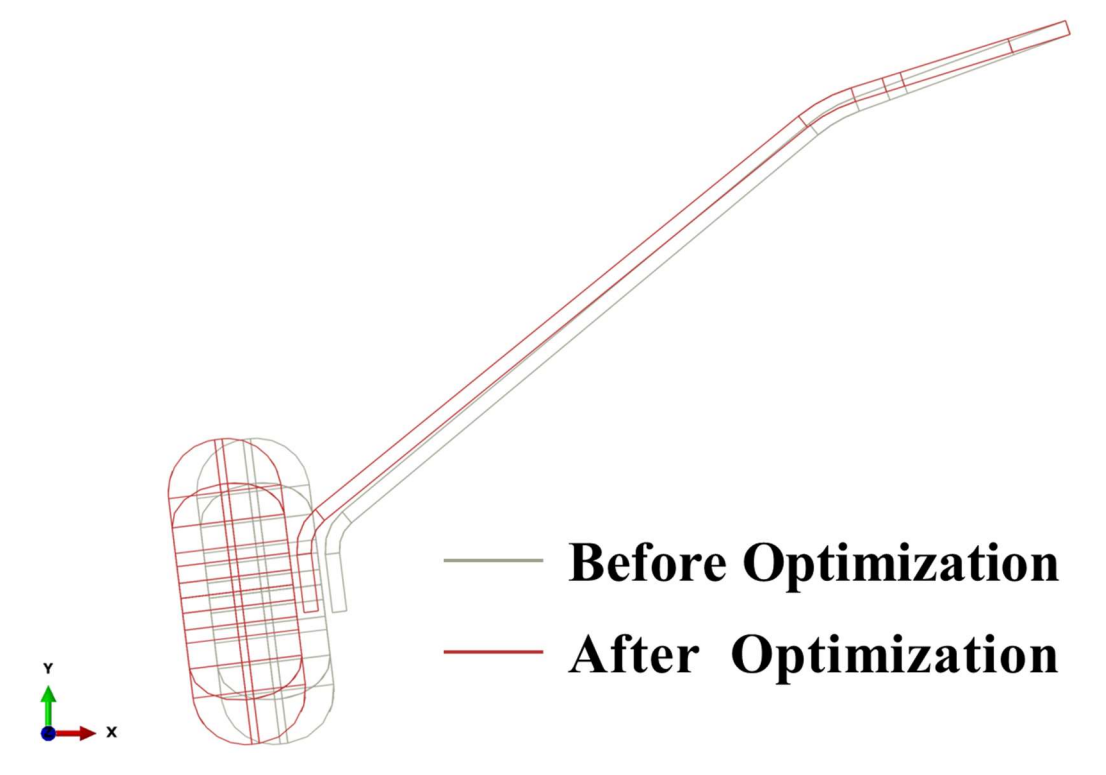


Figure 27 – Comparison of optimization results: iteration 144.

8. Conclusion

This study constructed a dynamic simulation model of landing impact process of leaf spring landing gear, which showed high reliability and accuracy. It provided reliable guidance for the overall design of landing gear and the structural design of buffer mechanisms.

This study used Python to develop the post-processing module of Abaqus and integrated the explicit dynamic simulation process of leaf spring landing gear with Isight for data extraction, analysis, calculation, and output, successfully achieving the automation of joint simulation—optimization process. The optimization process took 64 hours, with a total of 241 optimization iterations for four optimization objectives, producing a total of 240 feasible solutions, accounting for 99.59%. Among them, there are 46 Pareto frontier solutions, namely 46 sets of design parameters. According to engineering experience, design parameters that meet the design requirements can be directly selected from the Pareto frontier solution set.

The optimization performance of NSGA-II is notably pronounced. Using Iteration 144 as an example, comparative results demonstrate that, relative to landing gear designed using conventional engineering heuristics, the optimized landing gear achieves a significant enhancement in buffer efficiency, increasing from 0.40 to 0.53, an improvement of 32.50%, with only a minimal sacrifice in leaf spring mass. Moreover, the wheel load RF2_max is reduced from 16505.80 N to 15657.10 N, a decrease of 5.14%, while maintaining structural stresses at 1204.80 MPa, which is within permissible limits.

The results of the optimization demonstrate the rationality and effectiveness of the optimization model,

providing a reference for the design of this type of landing gear.

9. Acknowledgements

This work was supported by Shanxi Province Science and Technology Major Project (No. 202101120401007), Shanxi Province Graduate Student Scientific Research and Innovation Project (No. 2023KY162), Shanxi Province Key Research and Development Program (No. 2020XXX017), Shanxi Province Higher Education Teaching Reform Project: Exploration and Practice of Integrated Teaching in Computational Mechanics Curriculum System for New Engineering Subjects.

The financial contributions are gratefully acknowledged.

10. Contact Author Email Address

Hang Wang: wanghan@tyut.edu.cn

11. Copyright Statement

The authors confirm that they, and/or their company or organization, hold copyright on all of the original material included in this paper. The authors also confirm that they have obtained permission, from the copyright holder of any third party material included in this paper, to publish it as part of their paper. The authors confirm that they give permission, or have obtained permission from the copyright holder of this paper, for the publication and distribution of this paper as part of the ICAS proceedings or as individual off-prints from the proceedings.

DYNAMIC DROP SIMULATION OF THE MAIN LANDING GEAR OF A GENERAL AVIATION AIRCRAFT

References

- [1] Nie H., Wei X. Key technologies and development trends in the design of large civil aircraft. *Journal of Nanjing University of Aeronautics & Astronautics*. No. 4, pp 427-432, 2008.
- [2] Li D., Fan Z., Zhang Y., et al. Optimum design and experiment of composite leaf spring landing gear for electric aircraft. *Chinese Journal of Aeronautics*, Vol. 33, No. 10, pp 2649-2659, 2020.
- [3] Tugay B. Gürdal, Türkmen Halit S. Structural optimization of the landing gear of a mini-UAV. *12th AIAA/ISSMO Multidisciplinary Analysis and Optimization Conference, MAO*, Victoria, British Columbia, Canada, 2008.
- [4] Roskam J. Airplane design part IV: layout design of landing gear and systems. Roskam Aviation and Engineering Corporation, 1989.
- [5] Venkatesan M., Helmen Devaraj D. Design and analysis of composite leaf spring in light vehicle. *International Journal of Modern Engineering Research*, Vol. 2, No. 1, pp 213-218, 2012.
- [6] Yang X., Nie H., Wei X., et al. Study on the shock absorption performance of composite leaf spring landing gear for a certain model. *Aeronautical Computing Technique*, Vol. 48, No. 03, pp 107-110, 2018.
- [7] Krason W., Malachowski J. Multibody rigid models and 3D FE models in numerical analysis of transport aircraft main landing gear. *Bulletin of the Polish Academy of Sciences, Technical Sciences*, Vol. 63, No. 3, pp 745-757, 2015.
- [8] Zhang B., Song B., Mao Z., et al. Layout optimization of landing gears for an underwater glider based on particle swarm algorithm. *Applied Ocean Research*, Vol. 70, pp 22-31, 2018.
- [9] Srivathsa A., Adarsha S. S., Narayana M. V. B., et al. The dynamic characteristics of a non-linear main landing gear system of an aircraft during landing. *Vibroengineering PROCEDIA*, Vol. 30, No. 1-2, pp 97-102, 2020.
- [10]Lu J., Nie W., Ma Y., et al. Analysis nonlinear mechanical characteristics analysis of a UAV landing gear shock absorber. *Journal of Physics: Conference Series*, Vol. 1684, No. 1, pp 012131, 2020.
- [11]Pirooz M., Mirmahdi S. H., Khoogar A. R. Robust force and displacement control of an active landing gear for vibration reduction at touchdown and during taxiing. *SN Applied Sciences*, Vol. 3, No. 4, 2021.
- [12]Sonowal P., Pandey K. M., Sharma K. K. Design and static analysis of landing gear shock absorber of commercial aircraft. *Materials Today: Proceedings*, Vol. 45, No. 2, 2021.
- [13]ASTM Committee on Standards. *Standard specification for design and performance of a light sport airplane*. ASTM F2245-16C, ASTM International, Washington, D.C., USA, 2018.
- [14]Cheng C., Zhang H., Qiu X. A. Optimal design of tube spring landing gear based on impact energy. *Journal of Mechanical Design and Manufacturing Engineering*, Vol. 51, No. 04, pp 49-53, 2022.
- [15] Engineering Sciences Data Unit. Frictional and retarding forces on aircraft tyres. Vol. 71026, 1971.
- [16] Wang L., Xie H., Zhang L. Research on the full stress design method for leaf spring landing gear. *Mechanical Research & Application*, Vol. 28, No. 05, pp 22-25, 2015.
- [17]Zhang Z., Ding W., Ma H. Local stress analysis of a defective rolling bearing using an explicit dynamic method. *Advances in Mechanical Engineering*, Vol. 8, No. 12, pp 5356-5377, 2016.
- [18]Xu X., Ni C., Yan X. Time domain integration method for vibration testing based on combined Simpson's Integration. *Journal of Metrology*, Vol. 41, No. 06, pp 704-709, 2020.
- [19]Koch P. N., Evans J. P., Powell D. Interdigitation for effective design space exploration using Isight. *Structural and Multidisciplinary Optimization*, Vol 23, No.2, pp 111–126, 2002.
- [20]Li Z, Zheng L, Yan Z, et al. Optimization design of double-row tapered roller bearings based on Isight. *Mechanical Design and Manufacturing*, No. 11, pp 30-33, 2017.
- [21] Currey N S. Aircraft landing gear design: principles and practices. AIAA Education Series, 1988.
- [22] Gudmundsson S. General aviation aircraft design: applied methods and procedures. Butterworth-Heinemann, 2013.
- [23] Srinivas N, Deb K. Multi-objective optimization using nondominated sorting in genetic algorithms. *Evolutionary Computation*, Vol. 2, No.3, pp 221–248, 1994.
- [24]Deb K, Agrawal S, Pratap A, et al. A fast elitist non-dominated sorting genetic algorithm for multi-objective

DYNAMIC DROP SIMULATION OF THE MAIN LANDING GEAR OF A GENERAL AVIATION AIRCRAFT

optimization: NSGA-II. IEEE Transactions on Evolutionary Computation, Vol. 6, No. 2, pp 182-197, 2002.